# Roles of the Basic Metals La, Ba and Sr as Additives in $Al_2O_3$-supported Pd-based Three-Way Catalysts

Yuan Jing,[†] Gang Wang,[†] Kah Wei Ting,[†] Zen Maeno,[†] Kazumasa Oshima,[⊥] Shigeo Satokawa,[⊥] Shuhei Nagaoka,*[§] Ken-ichi Shimizu[†,‡], Takashi Toyao,*[†,‡]

[†] Institute for Catalysis, Hokkaido University, N-21, W-10, Sapporo 001-0021, Japan

[‡] Elements Strategy Initiative for Catalysts and Batteries, Kyoto University, Katsura, Kyoto 615-8520, Japan

[⊥] Department of Materials and Life Science, Faculty of Science and Technology, Seikei University, Musashino, Tokyo 180-8633, Japan

[§] Johnson Matthey Japan G.K., 5123-3, Kitsuregawa, Sakura, Tochigi 329-1412, Japan

Corresponding authors:
Takashi Toyao (toyao@cat.hokudai.ac.jp)
Shuhei Nagaoka (Shuhei.Nagaoka@mattheyasia.com)

## Abstract

Three-way catalytic converters are widely used to regulate emissions from gasoline-powered vehicles. Although significant effort over the past 40 years has resulted in the discovery of several metal additives that improve the thermal stability of three-way catalysts (TWCs), their effects on the actual catalytic process have not been studied systematically. The present work examined the roles of the typical basic metal additives La, Ba and Sr in Pd-based TWC systems, using various spectroscopic and kinetic studies. Metallic $Pd^0$ species on $Sr/Al_2O_3$ and $Ba/Al_2O_3$ supports were found to be more electron-rich compared with those on pristine $Al_2O_3$, whereas those on $La/Al_2O_3$ were more electron-deficient. Consequently, $Pd/La/Al_2O_3$ showed a lessened CO poisoning effect during NO reduction reactions. Evaluations were performed using powdered catalysts as well as monolithic honeycomb catalysts under conditions simulating actual use. $Pd/La/Al_2O_3$ was observed to promote the catalytic reduction of NO most efficiently, while $Pd/Ba/Al_2O_3$ exhibited the highest activity for the oxidations of CO and $C_3H_6$. The present data suggest that the optimal metal additive for a Pd-based TWC will be determined by the specific application. The selection of such metals should take into account not only the stability but also the promotional effect during the exhaust purification process.

## Keywords

Three-way catalysts, basic metals, *in situ*/*operando* spectroscopy, XAS

## 1. Introduction

Three-way catalysts (TWCs) provide an efficient means of reducing the pollutant emissions from gasoline-powered vehicles, by simultaneously removing compounds such as $NO_x$, CO and hydrocarbons (HCs) [1–3]. These catalysts are typically made of platinum group metals (PGMs), including Pt, Pd and Rh [4,5], because these elements exhibit superior catalytic performance and durability in comparison to nonprecious metals such as Cu, Ni and Fe [6–9]. As the regulatory requirements to reduce automotive emissions become increasingly strict, the development of effective support materials to improve the catalytic performance of PGMs is of great importance [10–13].

$Al_2O_3$ is widely used as a support material in TWCs because it has the advantages of possessing suitable mechanical strength, relatively good thermal stability and a high surface area [14,15]. Alkaline and alkaline earth metals as well as lanthanides are frequently combined with $Al_2O_3$ as structural stabilizers to suppress the transformation of $Al_2O_3$ from the $\gamma$ to $\alpha$ phase [16–21]. Certain basic metals, such as La and Ba, are also known to stabilize Pd species during thermal treatment, resulting in improved dispersion of the Pd [22–25]. However, to date, only limited studies have been conducted to investigate the promotional effect of these basic metal additives on the catalytic performances of TWCs [26–30]. As an example, Muraki and coworkers reported that the addition of

La promoted the $NO_x$ chemisorption, leading to the selective reduction of $NO_x$ rather than $O_2$, and also inhibited the HCs adsorption on Pd, resulting in more efficient reduction of $NO_x$ [31–34]. In addition, Sekiba et al confirmed that the introduction of $La_2O_3$ and BaO into a $Pd/CeO_2/Al_2O_3$ catalyst enhanced the catalytic performance of this material during NO conversion under reducing conditions [35]. Kobayashi and co-workers have also reported that the abilities of Pd-based catalysts to catalytically remove $NO_x$ were improved following the addition of basic elements, including La, Ba and Sr [36]. Prior reports such as these have suggested that the electron densities of Pd species are increased by the addition of these elements. Our own group recently reported work assessing the promotional effect of La in La-loaded $Al_2O_3$-supported Pd ($Pd/La/Al_2O_3$) catalysts serving as TWCs [37,38]. These prior studies demonstrated that metallic $Pd^0$ species in $Pd/La/Al_2O_3$ are more electron-deficient than those in $Pd/Al_2O_3$, which in turn suppresses the poisoning effect of CO and increases the catalytic activity for the removal of NO. Moreover, we reexamined the effective loading amount of La, which has conventionally been in the range of 3–5 wt%, with the aim of optimizing the specific surface area of the $La/Al_2O_3$ supports, and found that substantially increasing the La loading to 15 wt% provided a more effective TWC that was more reactive with NO, and suppressed the poisoning effect of CO. Although such work greatly contributed to the body of knowledge concerning TWCs, our present understanding of the roles of practically-used basic metal additives such as La, Ba or Sr in reactions over Pd-based catalysts remains insufficient. It would therefore be highly beneficial to systematically investigate the functions of such additives in TWCs especially under working conditions so as to develop efficient support materials that maximize the catalytic activity of Pd, which is the most commonly used active metal in modern commercial TWCs [39–41].

The present study performed a systematic investigation of the promotional effect of the basic metals La, Ba and Sr on the TWC process. A series of $Pd/M/Al_2O_3$ catalysts (M = La, Ba or Sr) was synthesized and these materials were investigated using various (*in situ*/*operando*) spectroscopic methods together with kinetics analyses. The results showed that metallic $Pd^0$ species loaded on $Ba/Al_2O_3$ and $Sr/Al_2O_3$ were more electron-rich than those on $Al_2O_3$, while the $Pd^0$ species on $La/Al_2O_3$ were more electron-deficient. The present data also indicated that $Pd/La/Al_2O_3$ promoted the catalytic reduction of NO most efficiently and that $Pd/Ba/Al_2O_3$ showed higher catalytic activity for the oxidations of $C_3H_6$ and CO.

## 2. Methods

### 2.1 Materials and Preparation of Catalysts

Chemicals were obtained from commercial suppliers and used as received. $La(NO_3)_3 \cdot 6H_2O$ (purity >99.0%), $Ba(OH)_2 \cdot 8H_2O$ (purity >97.0%), and $Sr(OH)_2 \cdot 8H_2O$ (purity >95.0%) were obtained from Kanto Chemical Co. A nitric acid aqueous solution containing $Pd(NH_3)_2(NO_2)_2$ (Pd content = 50.4 g $L^{-1}$, Nitric acid content = 66.9 g $L^{-1}$) was supplied by Kojima Chemicals. $\gamma$-$Al_2O_3$ (purity >97.5%) was obtained from Sasol. He (purity >99.995%), $H_2$ (purity >99.99%), $O_2$ (purity >99.5%), $N_2$ (purity >99.99%), Ar (purity >99.99%), NO (purity >99.5%), CO (purity >99.95%), $CO_2$ (purity >99.99%), $C_3H_6$ (purity >99.95%) gasses were obtained from Air Water Inc. and were used for catalyst preparations, catalytic reactions using powdered catalysts, and *in situ/operando* experiments. For catalysts aging under hydrothermal redox conditions and catalytic reactions using honeycomb catalysts, purities of gasses used are as follows; >99.9999% for $H_2$, >99.5% for $O_2$, >99.0% for NO, >99.9% for CO, >99.5% for $CO_2$, and 99.9999% for $C_3H_6$.

The introduction of basic metal (La, Ba, or Sr) to $\gamma$-$Al_2O_3$ was carried out as described in previous studies [37,38]. The basic-metal-loaded $Al_2O_3$ was dried at 120 °C for 2 h, followed by calcination in air at 600 °C for 2 h and were noted as $M/Al_2O_3$ (M = La, Ba, or Sr). Supported Pd (3wt % Pd) catalysts were prepared by an impregnation method as follows. 5 g of $M/Al_2O_3$ (or $Al_2O_3$) and 100 mL of aqueous solution containing 1.45 mmol (0.338 g) of $Pd(NH_3)_2(NO_2)_2$ were added to a glass vessel. The mixture was then stirred for 15 min (200rpm) at room temperature. After stirring, the mixture was evaporated to dryness at 50 °C under reduced pressure, dried at 90 °C for 12 h, and calcined in air at 300, 500 or 600 °C for 3h. Afterward, the calcined samples were pretreated under a flow of pure $H_2$ (20 mL $min^{-1}$) at 500 °C for 0.5 h in a Pyrex tube. The samples pretreated under the flow of pure $H_2$ (20 mL $min^{-1}$) were used for the characterization experiments unless otherwise stated. Before each catalytic activity test and *in situ/operando* experiments, the samples were reduced again under flowing 10%$H_2$/He (100 mL $min^{-1}$) at 400 °C for 0.5 h.

The slurry, which was composed of an inorganic binder, the calcined catalyst powders, and water, was coated onto a cordierite honeycomb (25.4 mmφ × 50 mm, 400 cells/$in^2$; NGK Insulators, Ltd.) to prepare the monolithic honeycomb catalysts. The thus prepared monolithic honeycomb catalysts were dried in air at 120 °C for 1h, followed by calcination at 600 °C for 2 h.

Monolithic honeycomb catalysts were aged at 1000 °C for 4 h under hydrothermal redox conditions. The gas compositions for rich (3% $H_2$, 3% CO, 10% $H_2O$, and $N_2$ balance), lean (3% $O_2$, 10% $H_2O$, and $N_2$ balance), and stoichiometric (10% $H_2O$ and $N_2$ balance) conditions were applied with intervals of 180 s for rich, 10 s for stoichiometric, 180 s for lean, and 10 s for stoichiometric atmospheres with flow rate = 3 L $min^{-1}$ (space velocity (SV) = 7,200 $h^{-1}$).

### 2.2 Catalyst Characterization

X-ray diffraction (XRD) patterns were measured using Cu-Kα radiation using Miniflex (Rigaku). $N_2$ adsorption measurements were conducted using AUTOSORB 6AG (Yuasa Ionics). High-angle annular dark-field scanning transmission electron microscopy (HAADF-STEM) images were collected using JEM-ARM200F (JEOL). CO adsorption experiments were performed at -20 °C using BELCAT (MicrotracBEL). It should be noted that the samples were pretreated under the flow of pure $H_2$ (20mL $min^{-1}$) at 500°C before these characterizations.

X-ray photoelectron spectroscopy (XPS) was performed on ESCA-3400HSE (Shimadzu), equipped with a modified UHV chamber using Mg Kα radiation. Binding energies were calibrated using the Al 2s peak of $Al_2O_3$ (119.5 eV). The reduced samples were measured using an Ar-filled glove box to avoid exposure of the samples to air.

### 2.3 (*Operando/in situ*) IR

*Operando* IR measurements were carried out at 150 °C using FT/IR-4200 (JASCO) with a Mercury-Cadmium-Telluride (MCT) detector. Samples (40 mg) were pressed to make pellets ($\phi$ = 20 mm), which were placed in the quartz IR cell having $CaF_2$ windows. The samples were heated under flowing 10% $H_2$/He (100 mL $min^{-1}$) at 400 °C for 0.5 h prior to the measurements. After cooling to 150 °C under flowing He, 0.5% NO/He was introduced for 10 min. After being purged by He for 10 min, 0.5% CO/He was introduced into the system for 10 min. The composition of the eluent was analyzed by a high-sampling-rate TCD GC (490 Micro GC; Agilent) and IR gas cell (JASCO FT/IR-4100). A reference spectrum, recorded at 150 °C under a flow of pure He, was subtracted from each spectrum.

The *in situ* IR measurements for CO adsorption was carried out at 40 °C by using the same apparatus described above. Prior to the adsorption experiments, the samples were exposed to 10% $H_2$/He (100 mL $min^{-1}$) for 30 min at 400 °C, followed by cooling to 40 °C under the flow of He. *In situ* IR spectra were collected after the introduction of 0.5% CO/He, followed by purge in the flow of He for 10 min.

### 2.4 (*Operando*) XAS

X-ray absorption spectroscopy (XAS) were performed in transmittance mode at the BL14B2 beamline of SPring-8 with a Si(311) double crystal monochromator. For measurements at the La, Ba and Sr K-edges, samples were sealed in polyethylene cells in air, and the spectra were measured at room temperature. For *operando* Pd K-edge XAS measurements, the high-sampling-rate TCD GC was employed for the analysis of $N_2$, $N_2O$, and CO. 150 mg of the samples in pellet form (φ: 10 mm) were added into a quartz cell with Kapton film windows. The catalyst was pretreated under a flow of 10% $H_2$/He (100 mL $min^{-1}$) at 400 °C for 0.5 h, followed by cooling to 150 °C. Subsequently, 0.5% NO/He, 0.5% CO/He, and 0.5%NO+0.5%CO/He (1000 mL $min^{-1}$) were introduced. The SV employed was ~ 30, 000 $h^{-1}$. The analysis was performed using Athena software ver. 0.9.25 included in the Demeter package [42]. The Fourier transformation of the $k^3$-weighted extended X-ray absorption fine structure

(EXAFS) was carried out over a *k* range of 3–12 $Å^{-1}$.

## 2.5 Catalytic Reactions

For the catalytic NO–CO reaction using the powdered catalysts, 15 mg of the catalyst was placed in a reactor using quartz wool in the catalyst bed. After the reduction of the catalyst under 10% $H_2$/He flow (100 mL $min^{-1}$) at 400°C for 0.5 h, the catalyst was cooled to 100 °C and the catalytic NO–CO reaction was started by supplying a gas mixture (0.5% CO, 0.5% NO, and He) at 100 mL·$min^{-1}$ (*W*/*F* corresponds to $1.5\times10^{-4}$ g·min·$cm^{-3}$). Products were analyzed by GC (Shimadzu GC-8A with a SHINCARBON ST column). The yields were calculated based on the following equation.

$$NO + CO \rightarrow 0.5\ N_2 + CO_2 \quad (1)$$

For the catalytic NO–$C_3H_6$ reaction using the powdered catalysts, a mixed gas containing 0.45% NO and 0.05% $C_3H_6$ (He balance) was fed to 15mg catalysts at 100 mL $min^{-1}$ (*W*/*F* corresponds to $1.5\times10^{-4}$ g·min·$cm^{-3}$) after the reduction under the flow of 10% $H_2$/He at 400°C for 0.5 h and cooling to 200 °C. The yield was calculated based on the following equation.

$$9NO + C_3H_6 \rightarrow 4.5\ N_2 + 3\ CO_2 + 3H_2O \quad (2)$$

For catalytic reactions on the honeycomb catalysts using MEXA-series (Horiba Ltd.), the catalysts were placed in a tubular-type reactor, and their catalytic performance was investigated by supplying a gas mixture containing NO, CO, $C_3H_6$, $O_2$, $H_2$, $CO_2$, $H_2O$, and $N_2$ balance at SV = 100,000 $h^{-1}$. Conversions of NO, CO, and $C_3H_6$, were monitored using a gas analyzer (ABB, AO-2020). Before each catalytic activity test, the honeycomb catalyst was pre-treated under a flow of the reaction gas (1 Hz perturbation between $\lambda$ = 0.95 and $\lambda$ = 1.05) at 400 °C for 0.5 h, followed by cooling to 100 °C under $N_2$. The $\lambda$ values were calculated according to the following equation (see **Tables 1** for detailed gas compositions).

$$\lambda = \frac{O_2 + 0.5CO + 0.5H_2O + CO_2 + 0.5NO}{0.5H_2 + CO + 1.5C_3H_6 + 0.5H_2O + CO_2} \quad (3)$$

**Table 1.** Composition of the simulated exhaust gas mixtures for TWC light-off tests.

| $\lambda$ | NO / % | CO / % | $C_3H_6$ / ppm | $O_2$ / % | $H_2$ / % | $CO_2$ / % | $H_2O$ / % | $N_2$ / % |
|---|---|---|---|---|---|---|---|---|
| 0.95 | 0.1 | 2.4 | 420 | 0.6 | 0.8 | 15 | 10 | balance |
| 1.00 | 0.1 | 0.6 | 420 | 0.6 | 0.2 | 15 | 10 | balance |
| 1.05 | 0.1 | 0.6 | 420 | 1.65 | 0.2 | 15 | 10 | balance |

## 3. Results and Discussion

### 3.1 Catalysts Characterization

The conditions used to prepare the $Pd/M/Al_2O_3$ and $Pd/Al_2O_3$ catalysts as well as the physicochemical properties of these materials are summarized in **Table 2**. We have employed higher Pd loading of 3 wt% in the present research than that used in the previous study (1 wt%) for ease of various measurements. Note that the 3 wt% Pd loading is within the range for the real-world applications. The loading amount of M was adjusted to be the same in the mol% (6.4, 10 and 10 wt% for Sr, Ba and La, respectively). The average Pd particle size in each catalyst was adjusted to approximately 6 nm by controlling the calcination temperature. $Pd/Al_2O_3$ was found to have a higher Brunauer–Emmett–Teller (BET) surface area compared with the $Pd/M/Al_2O_3$ series of samples in the as-prepared state (fresh). The XRD patterns provided in **Figure S1** demonstrate that each catalyst generated broad diffraction peaks attributable to $\gamma$-$Al_2O_3$. Peaks related to $BaCO_3$ and $SrCO_3$ were also present in the XRD patterns obtained from the $Pd/Ba/Al_2O_3$ and $Pd/Sr/Al_2O_3$ catalysts, respectively, confirming the presence of these carbonate species. These results are consistent with previous reports [37,38].

Characterization of the $M/Al_2O_3$ specimens using HAADF-STEM demonstrated that La, Ba and Sr were thoroughly dispersed on the atomic level over the $\gamma$-$Al_2O_3$ support (**Figure 1**). The data acquired from characterizations of the samples and of reference compounds using XAS at the La, Ba and Sr K edges are presented in **Figure S2**. Curve-fitting analyses of the EXAFS results are summarized in **Table S1**, and show that the spectrum of each $Pd/M/Al_2O_3$ specimen contained only a single M–O contribution. The results of M (M = La, Ba or Sr) K-edge XAS combined with the HAADF-STEM images indicated that La, Ba and Sr loaded on the $\gamma$-$Al_2O_3$ were highly dispersed and have a spatial uniformity of dopants dispersion, in agreement with reports based on earlier studies of similar materials [37,38,43–45].

**Table 2.** Preparation conditions and physicochemical characteristics of $Pd/Al_2O_3$ and $Pd/M/Al_2O_3$.

| Catalyst[a] | Loading amount of M | $T_{Calcination}$ / °C | $T_{H2\ reduction}$ / °C | $S_{BET}$ / $m^2\ g^{-1}$ | CO adsorbed[b] / $\mu mol\ g^{-1}$ | Particle size of Pd[c] / nm |
|---|---|---|---|---|---|---|
| $Pd/Al_2O_3$ | - | 600 | 500 | 155 | 52.6 | 6.0 |
| $Pd/Sr/Al_2O_3$ | 6.4 wt% | 500 | 500 | 146 | 51.9 | 6.1 |
| $Pd/Ba/Al_2O_3$ | 10 wt% | 300 | 500 | 139 | 47.8 | 6.5 |
| $Pd/La/Al_2O_3$ | 10 wt% | 500 | 500 | 134 | 55.1 | 5.7 |

[a]Pd loading amount = 3 wt%. [b]Measured at at -20 °C. [c]Estimated from the CO adsorption experiments.

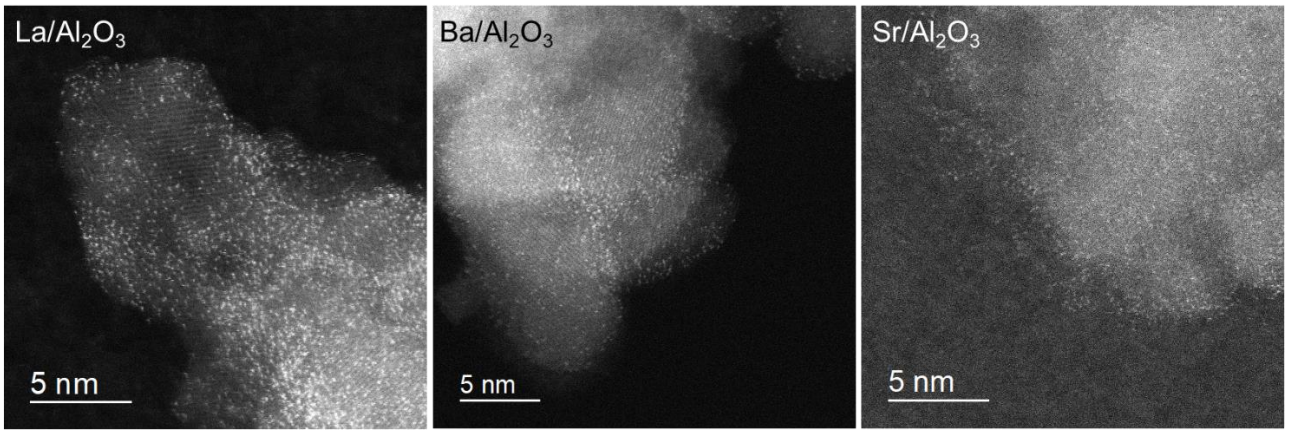

**Figure 1**. HAADF-STEM images of the $M/Al_2O_3$ (M = La, Ba or Sr) supports.

The electronic structures of the Pd nanoparticles in the $Pd/Al_2O_3$ and $Pd/M/Al_2O_3$ catalysts were assessed using IR spectroscopy in conjunction with CO adsorption as well as XPS. **Figure 2A** presents the *in situ* IR spectra acquired from the Pd catalysts following CO adsorption. In these spectra, the peak at approximately 2080 $cm^{-1}$ is attributed to CO molecules bound to the on-top sites of metallic surfaces [46]. The centers of the peaks generated by the $Pd/Ba/Al_2O_3$ and $Pd/Sr/Al_2O_3$ appeared at lower wavenumbers (2078 and 2080 $cm^{-1}$, respectively) compared with the peak produced by the $Pd/Al_2O_3$ (2082 $cm^{-1}$), whereas the peak in the $Pd/La/Al_2O_3$ spectrum was located at a higher wavenumber (2084 $cm^{-1}$). It is well known that the adsorption strength of CO on transition metals is mostly determined by the contribution from $\pi$ back-donation of transition metals to the CO $2\pi^*$ antibonding orbital, which is the lowest unoccupied molecular orbital (LUMO) [47,48]. The stronger the back-donation is, the weaker the C≡O bonds become, resulting in more activation of adsorbed CO molecules [49]. That is, in the present case, $\nu_{C=O}$ is weaker (red-shifted) when CO is adsorbed on negatively charged Pd due to the enhanced back-donation character of Pd to CO $2\pi*$ antibonding orbitals. Therefore, the metallic $Pd^0$ species supported on $Sr/Al_2O_3$ and $Ba/Al_2O_3$ were determined to be more electron-rich compared to those on pristine $Al_2O_3$, whereas those on $La/Al_2O_3$ were more electron-deficient.

**Figure 2B** provides Pd 3d XPS spectra obtained from the $Pd/Al_2O_3$ and $Pd/M/Al_2O_3$ specimens immediately after $H_2$ reduction, avoiding any subsequent exposure to air by using a glove box connected to the XPS sample chamber. These spectra include signals from both the $3d_{5/2}$ and $3d_{3/2}$ Pd core levels, and the $3d_{5/2}$ signal in the binding energy range of 335-336 eV can be assigned to metallic Pd [50–52]. Notably, the $3d_{5/2}$ signals generated by the $Pd/Sr/Al_2O_3$ (335.2 eV) and $Pd/Ba/Al_2O_3$ (335.3 eV) appeared at lower energies, while that produced by the $Pd/La/Al_2O_3$ (335.7 eV) was located at a higher energy compared with the result for the $Pd/Al_2O_3$ (335.5 eV). These data indicate that the $Pd^0$ species loaded on the $Ba/Al_2O_3$ and $Sr/Al_2O_3$ were more electron-rich but those on the $La/Al_2O_3$ were electron-poor relative to the $Pd/Al_2O_3$. Thus, the XPS spectra were consistent

with the results of the *in situ* IR analyses following CO adsorption.

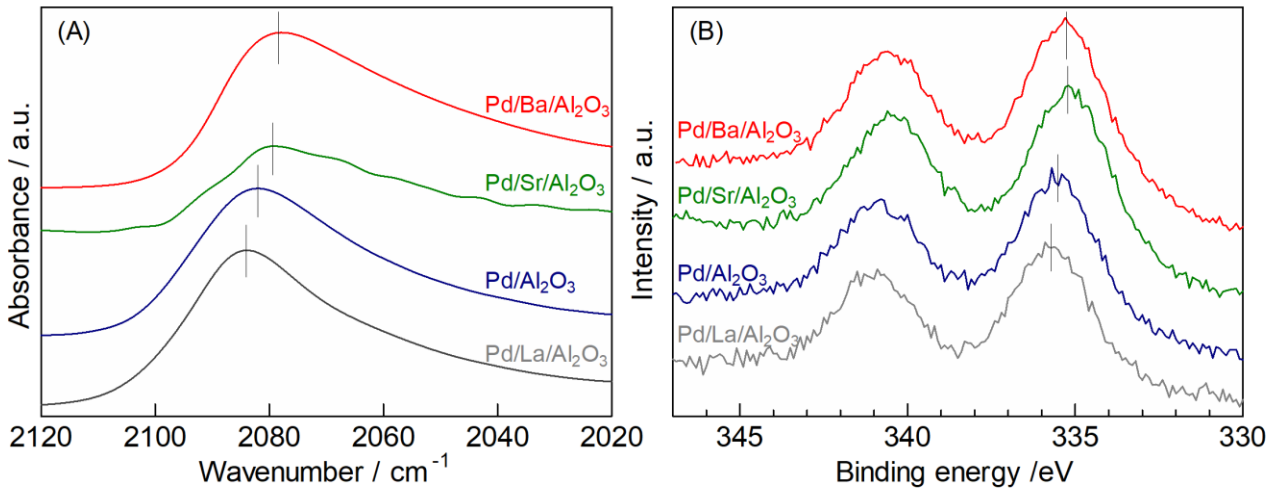


**Figure 2**. (A) *In situ* IR spectra of CO adsorbed on the $Pd/Al_2O_3$ and $Pd/M/Al_2O_3$ (M = La, Ba or Sr) catalysts. These spectra were collected under a flow of He following a 30 min exposure to CO. (B) Pd 3d XPS spectra for the $Pd/Al_2O_3$ and $Pd/M/Al_2O_3$ (M = La, Ba or Sr) catalysts. Spectra were obtained from the samples immediately after $H_2$ reduction without any exposure to air using a glove box connected to the XPS chamber.

### 3.2 Promotional Effect of the Basic Metal Additives on the NO Reduction Activity

**Figure 3(A)** summarizes the catalytic conversions of NO during the NO–CO reaction, which is a primary $DeNO_x$ reaction [53–56], over the $Pd/Al_2O_3$ and $Pd/M/Al_2O_3$ catalysts in powder form under steady state conditions. The complete reaction results are provided in **Figure S3** in the Supporting Information. The introduction of La, Ba or Sr evidently enhanced the catalytic conversions of both NO and CO, especially at low temperatures (below 250 °C). It should be noted that $N_2O$ and $CO_2$ were the main products in this low temperature region, and mass balance was 100% for all the temperature regime. Also, we have performed Weisz-Prater analysis [57] and confirmed that our activity tests were performed in the kinetic regimes. The catalytic activities of these materials, in terms of the conversions of both NO and CO, were found to decrease in the order of $Pd/La/Al_2O_3$ > $Pd/Ba/Al_2O_3$ > $Pd/Sr/Al_2O_3$ > $Pd/Al_2O_3$. In addition, the NO–$C_3H_6$ reaction, which is another important primary $DeNO_x$ reaction [58,59], were also carried out to study the effect of basic metal additives on the NO reduction activity (**Figure S4**). $Pd/Ba/Al_2O_3$ showed the highest NO conversion at 300 °C, followed by $Pd/La/Al_2O_3$ and $Pd/Sr/Al_2O_3$. The results indicate that the introductions of La, Ba or Sr are also effective for the NO–$C_3H_6$ reaction.

To further investigate the role of these metals in the NO–CO reaction, the effects of the CO concentration on the reaction rates over $Pd/Al_2O_3$ and the $Pd/M/Al_2O_3$ specimens were examined, with the results presented in **Figure 3(B)**. It should be noted that turnover frequency (TOF) based on reaction rates and amount of CO adsorbed (**Table 2**) were determined from the reaction data for NO conversions up to 30%. The apparent reaction orders based on these log-log plots with respect to CO were determined to be -0.50, -1.07, -1.00 and -0.94 over the $Pd/La/Al_2O_3$, $Pd/Ba/Al_2O_3$, $Pd/Sr/Al_2O_3$ and $Pd/Al_2O_3$, respectively. The negative values indicate that CO inhibited the NO–CO reaction over the catalysts used in the present study, in association with the strong adsorption of CO molecules on the surfaces of the supported Pd nanoparticles [60,61]. The apparent reaction order associated with the $Pd/La/Al_2O_3$ was more positive than that over the other catalysts, suggesting that the poisoning effect of CO was weakened following the introduction of La [37]. In contrast, the apparent reaction orders obtained for the $Pd/Ba/Al_2O_3$ and $Pd/Sr/Al_2O_3$ were more negative than that for the pristine $Pd/Al_2O_3$. The most probable explanation for these results is that electron-deficient $Pd^0$ species on the $La/Al_2O_3$ weakened the adsorption of CO molecules on the Pd surface, thus suppressing the poisoning effect of CO, whereas electron-rich $Pd^0$ species on the $Ba/Al_2O_3$ and $Sr/Al_2O_3$ enhanced this adsorption, thus promoting the poisoning effect. It should also be noted that the reduction in the CO poisoning effect obtained following La addition in the present study was less than that observed in previous work using $Pd/La/Al_2O_3$ with La and Pd loadings of 15 and 1 wt%, respectively. This discrepancy can presumably be ascribed to the larger Pd particle size resulting from the higher Pd loading of 3 wt% in the present research, which reduced the support effects to change the electronic properties of the supported Pd species.

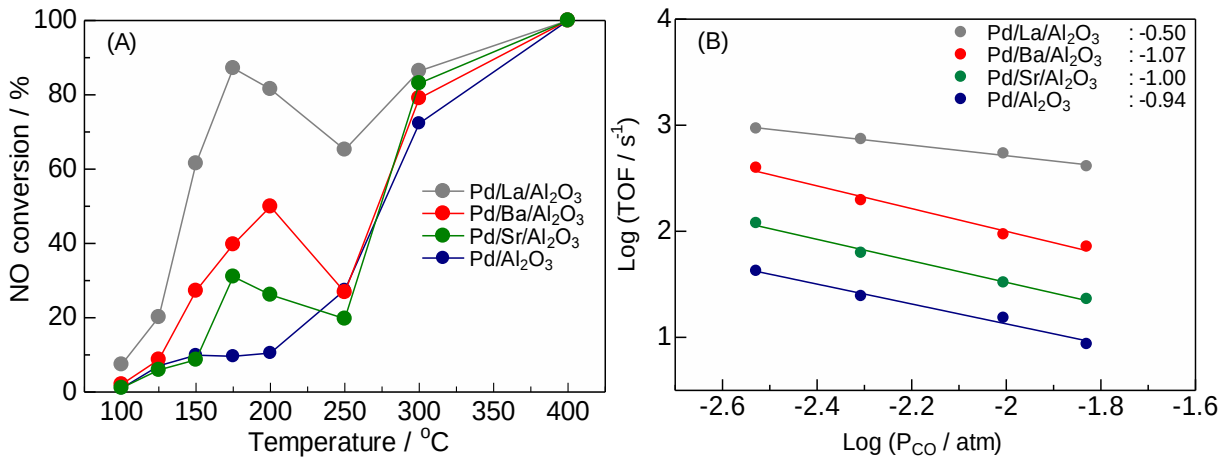


**Figure 3**. (A) Catalytic conversion of NO during the NO–CO reaction over the $Pd/Al_2O_3$ and $Pd/M/Al_2O_3$ (M = La, Ba or Sr) catalysts as fresh powders. Feed composition: 0.5% NO, 0.5% CO with He as the balance. (B) The log of the TOF as a function of the log of the CO concentration during the NO–CO reaction for each material. Conditions: 0.5% NO, 0.3-1.5% CO with He as the balance at 200 °C.

The effects of these metal additives on the chemical states of Pd during the NO–CO reaction were further investigated by performing *operando* Pd K-edge XAS analyses [62,63] under 0.5% NO/He, 0.5% CO/He or 0.5%NO+0.5%CO/He flows at 200 °C. Prior to analysis, each sample was pre-reduced at 500 °C under a flow of 10% $H_2$/He, and then reduced again in the XAS cell under 10% $H_2$/He at 400 °C just prior to the experiment. The *operando* Pd K-edge X-ray absorption near-edge structure (XANES) data and the FT of the $k^3$-weighted EXAFS spectra acquired under a 0.5% NO/He flow are shown in **Figures 4 and S5**. Note that the $Pd/La/Al_2O_3$ spectra are included in the main text as representative data. In each case, the absorption edge positions gradually shifted to higher energies following exposure to NO, while the intensity of the FT peak corresponding to Pd–Pd bonds (at approximately 2.5 Å) decreased. These results demonstrate that the Pd in these materials was oxidized by the NO. It was also found that no Pd–O contribution was seen in the FT of the $k^3$-weighted EXAFS spectra of $Pd/Al_2O_3$, which is in accordance with our previous study [37]. This lack of evidence for Pd–O bonds is attributed to the formation of oxidized and highly dispersed Pd species, which do not generate PdO species with well-defined Pd–O bonds. Similar phenomena have been reported for related materials [64–67]. In contrast, a Pd–O contribution was observed in the $Pd/M/Al_2O_3$ spectra, especially those of the $Pd/La/Al_2O_3$ and $Pd/Ba/Al_2O_3$. This finding reflects the strong anchoring effects of La and Ba, which would be expected to limit the deactivation of Pd species under the harsh TWC reaction conditions [24,25].

During these oxidation trials, $N_2O$ was formed as the gas phase product and was monitored using a gas chromatograph with a thermal conductivity detector operating at a high sampling rate (**Figure 4C**). The $Pd^0$ fraction ($Pd^0/(Pd^0+Pd^{II})$) obtained from linear combination fitting of the XANES data indicated that the Pd species were oxidized by the NO introduced into the system (**Figure 4D**). Thirty

minutes after the introduction of NO, the $Pd^0$ fraction was determined to be 0.71 in the case of the $Pd/La/Al_2O_3$, which exhibited the highest level of oxidation among the four catalysts that were tested. After a He purge to remove residual gaseous NO, CO was introduced such that the partly oxidized Pd species were reduced with the simultaneous formation of $N_2O$ and a small amount of $CO_2$. The results demonstrated that surface-adsorbed $NO_x$ species that had been generated upon exposure to NO and retained during the He purge served as the source of $N_2O$. The incorporation of the basic metal additives evidently promoted the oxidation of Pd with decreasing effect in the order of La > Ba > Sr. It is also worth noting that the formation of $CO_2$ was observed along with the reduction of partially oxidized species. Based on these results, it is apparent that the NO–CO reaction over supported Pd catalysts comprises a redox cycle involving Pd species with NO as an oxidant and CO as a reductant.

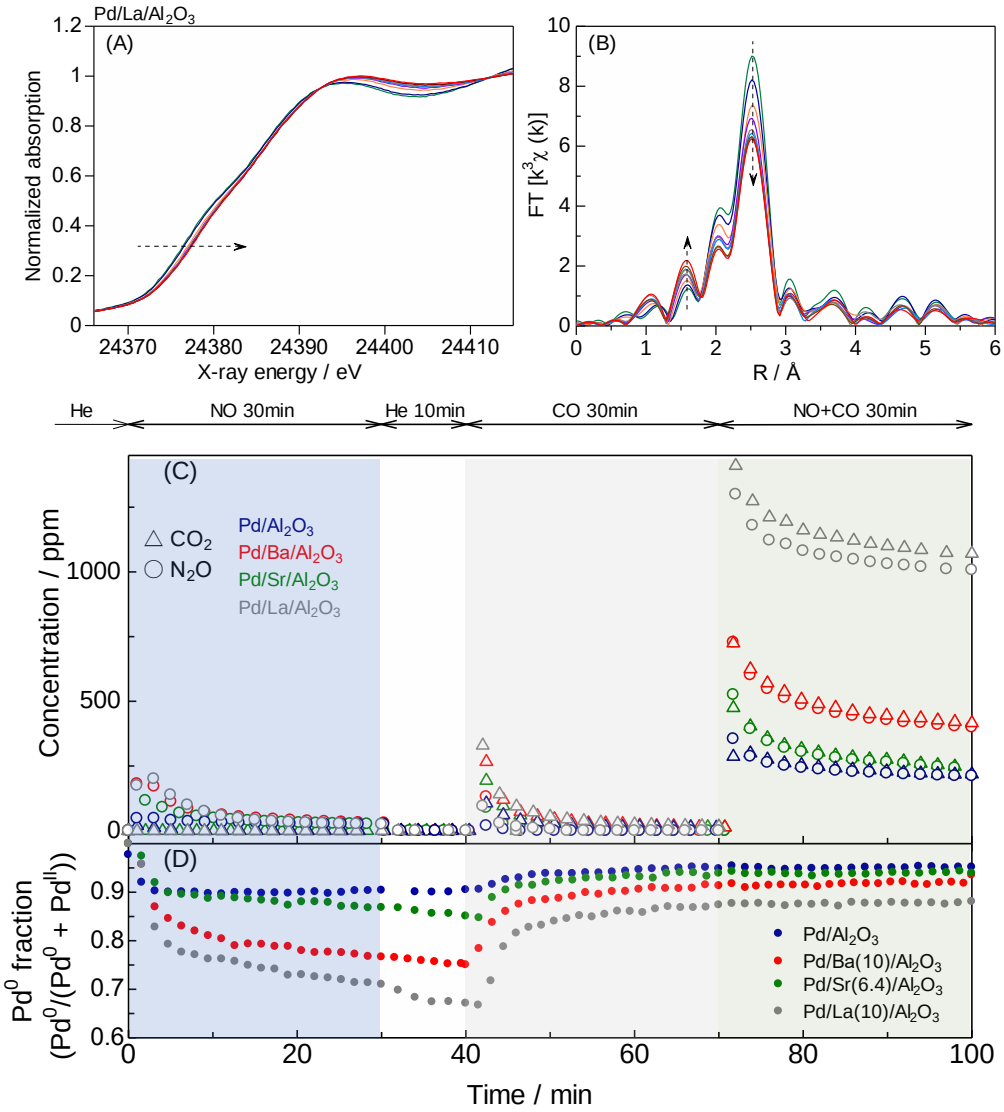


**Figure 4**. Results of the *operando* Pd K-edge XAS analyses. Pd K-edge (A) XANES spectra and (B) $k^3$-weighted EXAFS FTs for $Pd/La/Al_2O_3$, acquired under flowing 0.5% NO/He (1000 mL $min^{-1}$) at 150 °C after the pretreatment. Changes in (C) the product concentrations in the gas phase and (D) the fraction of $Pd^0$ under NO, CO and NO+CO flows at 150 °C.

*Operando* IR data were acquired to assess the roles of La, Ba and Sr in the formation of surface adsorbed species as well as the reactivities of these metals during the NO reduction. The results are provided in **Figure 5**. These spectra were collected under a flow of He after the introduction of 0.5% NO/He for 30 min followed by a flow of 0.5% CO/He. Subsequent to exposure to NO, various $NO_x$ species were produced on the surfaces of the catalysts, as reflected in the peaks that appeared in the 1100–1700 $cm^{-1}$ region [68–70]. Specifically, the peaks at 1191 and 1232 $cm^{-1}$ are attributed to surface nitrite species [38,71,72]. The intensities of these peaks in the spectra of each $Pd/M/Al_2O_3$ specimen were higher than that generated by the $Pd/Al_2O_3$, indicating that the introduction of La, Ba or Sr promoted the formation of surface nitrite species more efficiently. The absorption bands in the 1250-1650 $cm^{-1}$ region are due to the presence of nitrate species with different adsorption modes [38,73–75]. The band at around 1660 $cm^{-1}$ is assigned to Pd-adsorbed NO species [38,76,77]. Considering that the *operando* XAS data demonstrated that $N_2O$ was formed when solely NO was introduced, it is believed that the disproportionation reaction of NO occurred to produce both gaseous $N_2O$ and surface nitrite species on the $Pd/M/Al_2O_3$. It is also important to note that the peaks obtained from the $Pd/M/Al_2O_3$ samples were essentially absent in the spectra generated by the $M/Al_2O_3$ without Pd (shown in seagreen), indicating the importance of combining Pd and $M/Al_2O_3$ as supports.

During the subsequent exposures of the $Pd/Al_2O_3$ and $Pd/M/Al_2O_3$ series to a flow of 0.5% CO/He, two strong peaks appeared at approximately 1560 and 1360 $cm^{-1}$ that are attributed to carbonate adsorbed on the catalyst surfaces [78]. After the introduction of CO, the intensities of the peaks related to nitrite species on the $Pd/M/Al_2O_3$ samples decreased. As demonstrated in **Figure 5B**, the intensities of these peaks in the $Pd/La/Al_2O_3$ spectra declined more rapidly than in the $Pd/Ba/Al_2O_3$ and $Pd/Sr/Al_2O_3$ spectra, indicating that nitrites on the $Pd/La/Al_2O_3$ were more reactive with CO. Simultaneous with the decline in surface nitrite species, higher concentrations of $N_2O$ and $CO_2$ were formed on the $Pd/La/Al_2O_3$ than on the $Pd/Ba/Al_2O_3$ and $Pd/Sr/Al_2O_3$, as shown in **Figure 5C**. This trend is in agreement with the results obtained during the catalytic NO–CO reaction trials described above. These data confirm that the efficient formation of nitrites and the reactivity of these species with CO played important roles in promoting the NO–CO reaction.

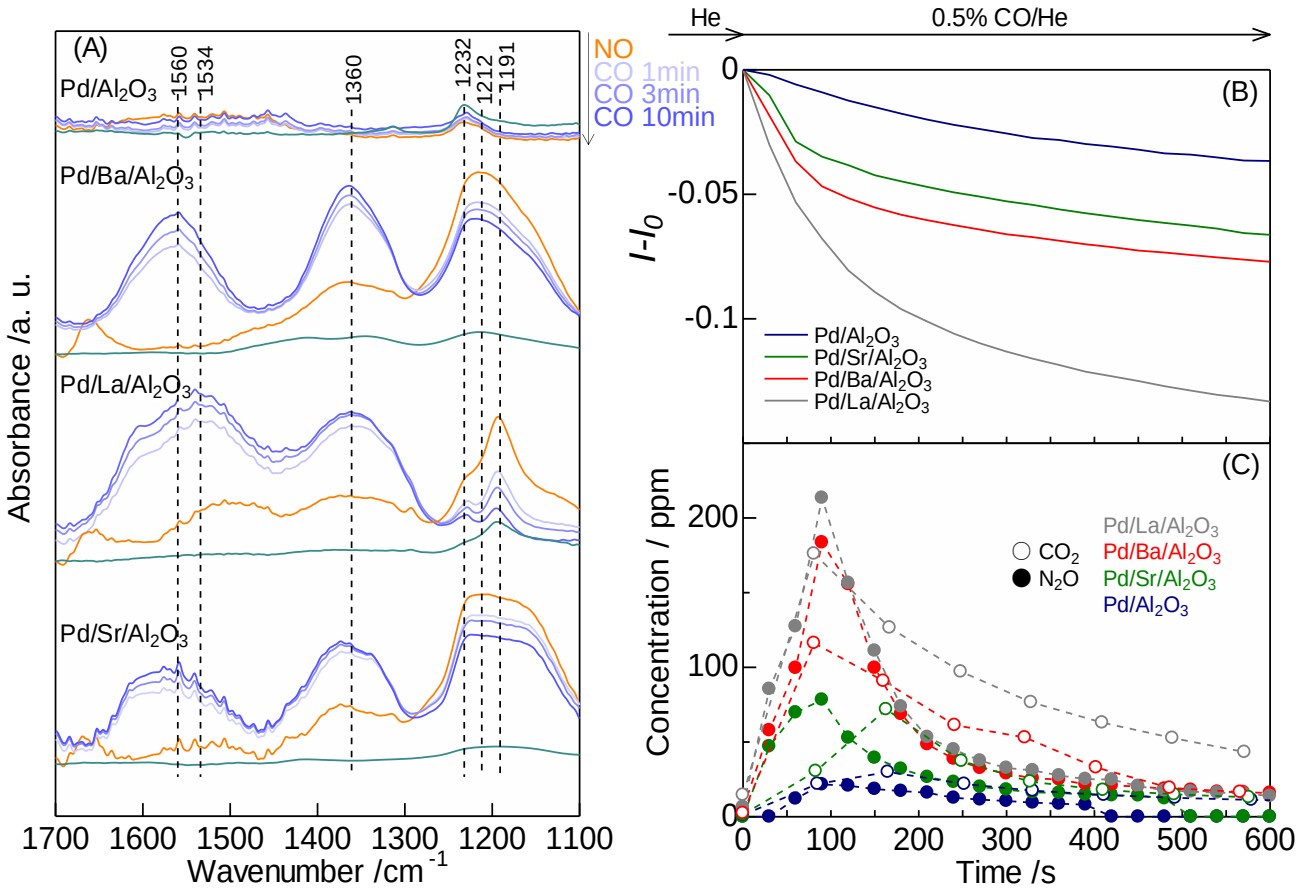


**Figure 5**. (A) *Operando* IR spectra showing the evolution of surface species adsorbed on the $Pd/Al_2O_3$ and $Pd/M/Al_2O_3$ (M = La, Ba or Sr) as well as the supports without Pd at 150 °C. The orange ($Pd/Al_2O_3$ and $Pd/M/Al_2O_3$) and seagreen ($Al_2O_3$ and $M/Al_2O_3$) spectra were collected under a flow of He after exposure to NO for 10 min. Subsequently, 0.5% CO/He was introduced into the cell in trials with the $Pd/Al_2O_3$ and $Pd/M/Al_2O_3$ and spectra were continuously acquired with simultaneous analysis of the gas phase products. Variations in (B) the intensities of peaks related to surface nitrite species and (C) the concentrations of $N_2O$ and $CO_2$ in the effluent gas upon the introduction of 0.5% CO/He.

### 3.3 Catalytic activity test using honeycomb catalysts under TWC condition.

The results of TWC light-off tests over the honeycomb catalysts are shown in **Figure 6**. The fresh monolithic Pd/M/$Al_2O_3$ exhibited higher NO conversion than the Pd/$Al_2O_3$, suggesting that the basic metal additives enhanced the ability of these honeycomb materials to remove NO from automotive emissions under TWC conditions. In addition, the La-loaded catalyst exhibited a higher degree of NO conversion in comparison with the others, in agreement with the NO–CO reaction data and corresponding *operando* XAS and IR results. In contrast, throughout the $C_3H_6$ and CO oxidation trials, the Ba-loaded sample showed higher CO and $C_3H_6$ conversions relative to the materials incorporating Sr and La. Ba is known to provide exceptional performance when added to Pd/$Al_2O_3$ catalysts intended for the oxidation of HCs such as methane, especially in the presence of water vapor [23,79,80]. This promotional effect has been attributed to electron donation from the Ba to the Pd on the support, in agreement with the findings of the present study.

The stability of these honeycomb catalysts was investigated using aged catalysts that were exposed to hydrothermal redox conditions. Information concerning stability is vitally important with regard to real-world applications of these catalysts because they will be exposed to harsh conditions in association with dynamic changes in temperature and ambient atmosphere during use [81–83]. It is also important to note that the hydrothermal aging of such materials, as an aspect of TWC research, must be conducted under varying lean/stoichiometric/rich conditions to simulate the actual operating conditions [84,85]. Although the conversions of NO, CO and $C_3H_6$ over each of the catalysts decreased after the aging treatment, the aged Pd/M/$Al_2O_3$ catalysts still exhibited higher catalytic performance than the aged Pd/$Al_2O_3$. The data also indicated that La was the most effective additive in terms of NO conversion, while Sr and Ba promoted the oxidations of $C_3H_6$ and CO to the greatest extent. Again, the high oxidation activities observed following the addition of these electron-donating basic metals are in good agreement with previous studies in which the oxidations of HCs were examined using Pd/$Al_2O_3$ catalysts modified with these elements [79,80].

The aged catalysts were characterized by XRD and $N_2$ adsorption techniques as shown in **Figure 7**. Note that the powder catalysts were subjected to the hydrothermal aging treatment for these measurements. Sharp peaks related to metallic Pd were observed in each of the XRD patterns, indicating that the Pd nanoparticles had aggregated into large particles that were detectable by XRD during aging. Peaks attributed to $BaAl_2O_4$ and $SrAl_2O_4$ were also observed in the XRD patterns obtained from the aged Pd/Ba/$Al_2O_3$ and Pd/Sr/$Al_2O_3$, respectively, whereas the XRD pattern generated by the aged Pd/La/$Al_2O_3$ showed no peaks assignable to $LaAlO_3$. In addition, $\alpha$-$Al_2O_3$ peaks appeared in the pattern of the aged Pd/$Al_2O_3$, suggesting a phase transformation from $\gamma$-$Al_2O_3$ to $\alpha$-$Al_2O_3$. Conversely, the aged Pd/M/$Al_2O_3$ materials were comprised mainly of $\gamma$-$Al_2O_3$, with no evidence of $\alpha$-$Al_2O_3$ being formed. The Sr, Ba, and La K-edge EXAFS FTs for the aged materials are shown in **Figure S6**. Results of the curve fitting analysis of EXAFS summarized in **Table S2** show that the aged

$Pd/Sr/Al_2O_3$ and $Pd/Ba/Al_2O_3$ catalysts only contained M–O contribution, and the aged $Pd/La/Al_2O_3$ catalyst comprises both La–O and slight La–(O)–Al contribution. The $S_{BET}$ values for both the fresh and aged catalysts are given in **Figure 7B**. These data show that the $Pd/M/Al_2O_3$ specimens retained high surface areas during the aging. Therefore, the addition of basic metals appears to have enhanced the thermal stability of the $Al_2O_3$ in these materials. These results are in agreement with previous reports of research focused on improving the thermal stability of $Al_2O_3$ by using basic metal additives as modifiers [18].

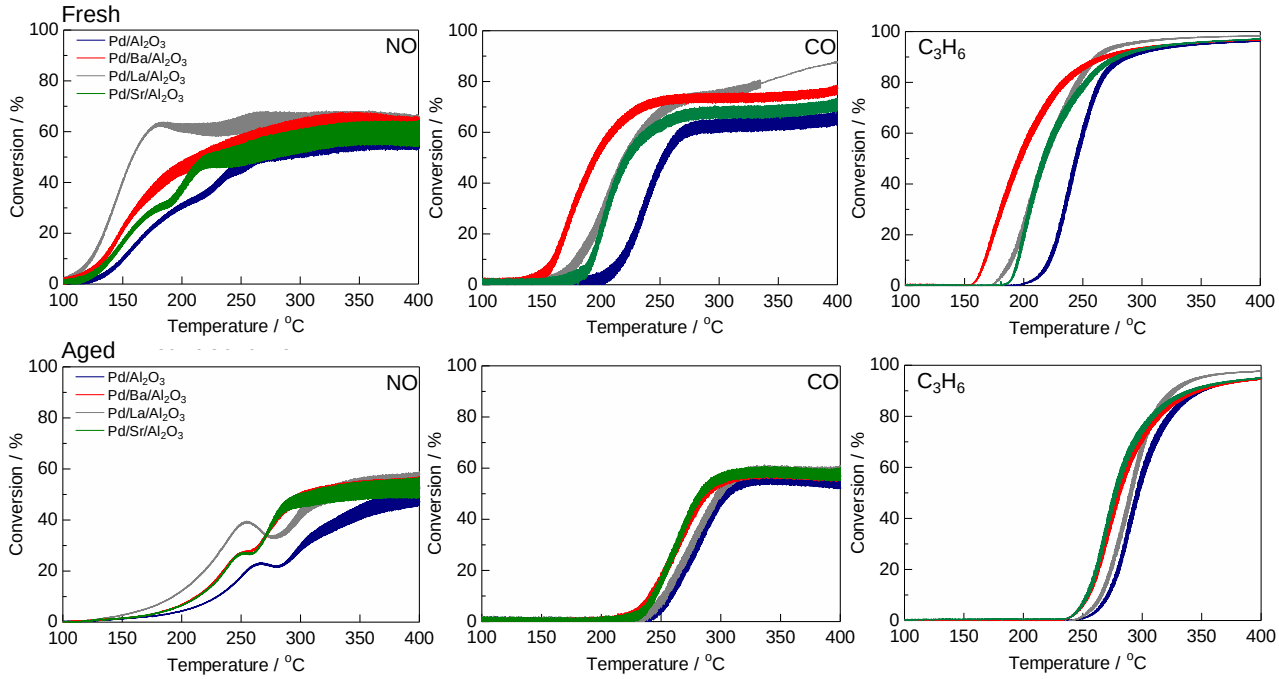


**Figure 6**. The conversions of NO, CO and $C_3H_6$ during TWC light-off tests over fresh and aged $Pd/Al_2O_3$-and $Pd/M/Al_2O_3$-coated honeycomb catalysts under gases perturbed at 1 Hz between $\lambda$ = 0.95 and $\lambda$ = 1.05. Heating rate: 25 °C/min; Gases: NO (0.1%), CO (2.4-0.6%), $C_3H_6$ (420 ppm), $O_2$ (0.6-1.65%), $H_2$ (0.8%), $CO_2$ (15%), $H_2O$ (10%), $N_2$ balance; SV = 100,000 $h^{-1}$.

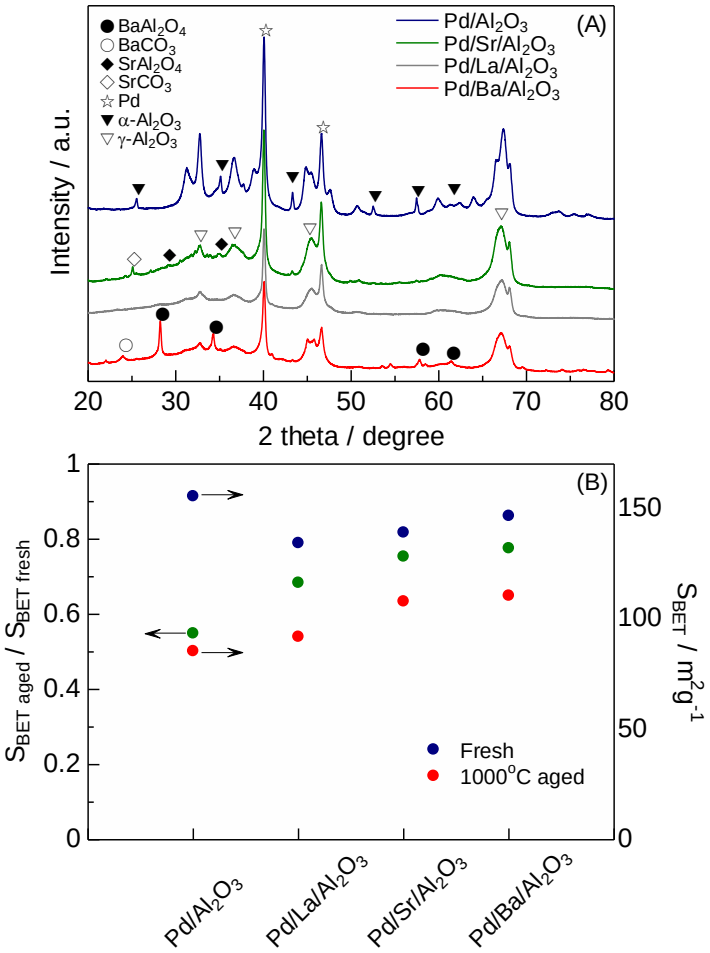


**Figure 7**. (A) XRD patterns obtained from aged $Pd/Al_2O_3$ and $Pd/M/Al_2O_3$ (M = La, Ba or Sr). (B) $S_{BET}$ values of fresh ($S_{BET\ fresh}$) and aged ($S_{BET\ aged}$) $Pd/Al_2O_3$ and $Pd/M/Al_2O_3$ (M = La, Ba or Sr) and the ratios of $S_{BET\ aged}$ to $S_{BET\ fresh}$.

## Conclusions

In this study, we examined the role of basic metal additives in $Pd/M/Al_2O_3$ (M = La, Ba or Sr) during the three-way catalytic process, using spectroscopic and kinetic measurements. Those catalysts loaded with the basic metals (the $Pd/M/Al_2O_3$ series) exhibited enhanced catalytic activity during the conversions of NO and CO. In addition, metallic Pd nanoparticles supported on $La/Al_2O_3$ were found to have a decreased electron density, such that the CO poisoning effect was suppressed. Conversely, Pd supported on $Sr/Al_2O_3$ and $Ba/Al_2O_3$ showed increased electron density. The presence of the atomically dispersed basic metals promoted the efficient formation of surface nitrite species, such that the $DeNO_x$ activity of the powdered catalysts was improved. Honeycomb-type monolithic catalysts were also prepared and their performance was examined under simulated TWC conditions. The results showed that the $Pd/M/Al_2O_3$ catalysts were superior in terms of promoting the reactions of NO, CO and $C_3H_6$ compared with the $Pd/Al_2O_3$ catalyst. $Pd/La/Al_2O_3$ was found to enhance NO reduction to a greater extent than the catalysts investigated in this work, while $Pd/Ba/Al_2O_3$ demonstrated superior catalytic performance during the oxidation of CO and $C_3H_6$.

**ACKNOWLEDGEMENTS**

This study was supported by KAKENHI (20H02775, 20H02518, 20KK0111, and 20F20345), “Integrated Research Consortium on Chemical Sciences (IRCCS)”, “Elements Strategy Initiative to Form Core Research Center” (JPMXP0112101003), and the JST-CREST project JPMJCR17J3. G.W. acknowledges a JSPS postdoctoral fellowship (No. P20345). The authors thank the technical division of Institute for Catalysis for manufacturing experimental equipment. XAS measurements were conducted at the BL-14B2 beamline of SPring-8 (2019B1686 and 2020A1695).

## References


[1] J. Wang, H. Chen, Z. Hu, M. Yao, Y. Li, A Review on the Pd-Based Three-Way Catalyst, Catal. Rev. 57 (2015) 79–144. http://www.tandfonline.com/doi/abs/10.1080/01614940.2014.977059.

[2] S. Matsumoto, Recent advances in automobile exhaust catalysts, Catal. Today. 90 (2004) 183–190.

[3] M. Shelef, R.W. McCabe, Twenty-five years after introduction of automotive catalysts: what next?, Catal. Today. 62 (2000) 35–50.

[4] S. Rood, S. Eslava, A. Manigrasso, C. Bannister, Recent advances in gasoline three-way catalyst formulation: A review, Proc. Inst. Mech. Eng. Part D J. Automob. Eng. 234 (2020) 936–949. doi:10.1177/0954407019859822.

[5] T. Zheng, B. Lu, G. Harle, D. Yang, C. Wang, Y. Zhao, A comparative study of Rh-only, Pd-only and Pd/Rh catalysts, Appl. Catal. A Gen. 602 (2020) 117649. doi:10.1016/j.apcata.2020.117649.

[6] S. Hosokawa, K. Matsuki, K. Tamaru, Y. Oshino, H. Aritani, H. Asakura, K. Teramura, T. Tanaka, Selective reduction of NO over $Cu/Al_2O_3$: Enhanced catalytic activity by infinitesimal loading of Rh on $Cu/Al_2O_3$, Mol. Catal. 442 (2017) 74–82. doi:10.1016/j.mcat.2017.09.005.

[7] T. Hirakawa, Y. Shimokawa, W. Tokuzumi, T. Sato, M. Tsushida, H. Yoshida, S. Hinokuma, J. Ohyama, M. Machida, Multicomponent Spinel Oxide Solid Solutions: A Possible Alternative to Platinum Group Metal Three-Way Catalysts, ACS Catal. 9 (2019) 11763−11773. doi:10.1021/acscatal.9b03772.

[8] K. Ueda, M. Tsuji, J. Ohyama, A. Satsuma, Tandem Base-Metal Oxide Catalyst: Superior NO Reduction Performance to the Rh Catalyst in $NO\text{-}C_3H_6\text{-}CO\text{-}O_2$, ACS Catal. 9 (2019) 2866−2869. doi:10.1021/acscatal.9b00526.

[9] J. Ohyama, J. Shibano, A. Satsuma, R. Fukuda, Y. Yamamoto, S. Arai, T. Shishido, H. Asakura, S. Hosokawa, T. Tanaka, Quantum Chemical Computation-Driven Development of Cu-Shell-Ru-Core Nanoparticle Catalyst for NO Reduction Reaction, J. Phys. Chem. C. 123 (2019) 20251–20256. doi:10.1021/acs.jpcc.9b03687.

[10] D.Y. Yoon, Y.J. Kim, J.H. Lim, B.K. Cho, S.B. Hong, I.S. Nam, J.W. Choung, Thermal stability of Pd-containing $LaAlO_3$ perovskite as a modern TWC, J. Catal. 330 (2015) 71–83. doi:10.1016/j.jcat.2015.07.013.

[11] R.J. Farrauto, M. Deeba, S. Alerasool, Gasoline automobile catalysis and its historical journey to cleaner air, Nat. Catal. 2 (2019) 603–613. doi:10.1038/s41929-019-0312-9.

[12] M. V. Twigg, Catalytic control of emissions from cars, Catal. Today. 163 (2011) 33–41. doi:10.1016/j.cattod.2010.12.044.

[13] L. Li, N. Zhang, R. Wu, L. Song, G. Zhang, H. He, Comparative Study of Moisture-Treated $Pd@CeO_2/Al_2O_3$ and $Pd/CeO_2/Al_2O_3$ Catalysts for Automobile Exhaust Emission Reactions: Effect of Core-Shell Interface, ACS Appl. Mater. Interfaces. 12 (2020) 10350–10358. doi:10.1021/acsami.9b20734.

[14] M. Machida, Y. Uchida, Y. Ishikawa, S. Hinokuma, H. Yoshida, J. Ohyama, Y. Nagao, Y. Endo, K. Iwashina, Y. Nakahara, Thermostable Rh Metal Nanoparticles Formed on $Al_2O_3$ by High-Temperature

$H_2$ Reduction and Its Impact on Three-Way Catalysis, J. Phys. Chem. C. 123 (2019) 24584−24591. doi:10.1021/acs.jpcc.9b06657.

[15] C. Huang, W. Shan, Z. Lian, Y. Zhang, H. He, Recent advances in three-way catalysts of natural gas vehicles, Catal. Sci. Technol. 10 (2020) 6407–6419. doi:10.1039/d0cy01320j.

[16] H. Arai, M. Machida, Thermal stabilization of catalyst supports and their application to high-temperature catalytic combustion, Appl. Catal. A Gen. 138 (1996) 161–176. doi:10.1016/0926-860X(95)00294-4.

[17] J.H. Kwak, J. Hu, A. Lukaski, D.H. Kim, J. Szanyi, C.H.F. Peden, Role of pentacoordinated $Al^{3+}$ ions in the high temperature phase transformation of γ-$Al_2O_3$, J. Phys. Chem. C. 112 (2008) 9486–9492. doi:10.1021/jp802631u.

[18] R. Di Monte, P. Fornasiero, J. Kaspar, M. Graziani, J.M. Gatica, S. Bernal, A. Gomez-Herrero, Stabilisation of nanostructured $Ce_{0.2}Zr_{0.8}O_2$ solid solution by impregnation on $Al_2O_3$: A suitable method for the production of thermally stable oxygen storage/release promoters for three-way catalysts, Chem. Commun. (2000) 2167–2168. doi:10.1039/b006674p.

[19] Y. Nishio, M. Ozawa, Thermal stability and microstructural change of lanthanum modified alumina catalytic support, J. Ceram. Soc. Japan. 115 (2007) 633–636.

[20] A.A. Vedyagin, R.M. Kenzhin, M.Y. Tashlanov, E.A. Alikin, V.O. Stoyanovskii, P.E. Plyusnin, Y. V. Shubin, I. V. Mishakov, M.Y. Smirnov, A. V. Kalinkin, V.I. Bukhtiyarov, Effect of La Addition on the Performance of Three-Way Catalysts Containing Palladium and Rhodium, Top. Catal. 63 (2020) 152–165. doi:10.1007/s11244-019-01213-x.

[21] T. Kolli, U. Lassi, K. Rahkamaa-Tolonen, T.J.J. Kinnunen, R.L. Keiski, The effect of barium on the catalytic behaviour of fresh and aged Pd-Ba-OSC/$Al_2O_3$ catalysts, Appl. Catal. A Gen. 298 (2006) 65–72. doi:10.1016/j.apcata.2005.09.019.

[22] S. Suhonen, M. Valden, M. Pessa, A. Savimäki, M. Härkönen, M. Hietikko, J. Pursiainen, R. Laitinen, Characterization of alumina supported Pd catalysts modified by rare earth oxides using X-ray photoelectron spectroscopy and X-ray diffraction: Enhanced thermal stability of PdO in Nd/Pd catalysts, Appl. Catal. A Gen. 207 (2001) 113–120. doi:10.1016/S0926-860X(00)00621-9.

[23] F. Klingstedt, H. Karhu, A. Kalantar Neyestanaki, L.E. Lindfors, T. Salmi, J. Väyrynen, Barium promoted palladium catalysts for the emission control of natural gas driven vehicles and biofuel combustion systems, J. Catal. 206 (2002) 248–262. doi:10.1006/jcat.2001.3505.

[24] M. Takahashi, S. Kikuchi, K. Iwachido, M. Ikeda, H. Goto, Development of New Three-way Catalyst Technologies to Improve Purification Performance for Exhaust Emission after Severe Thermal Aging, Trans. Soc. Automot. Eng. Japan. 44 (2013) 15–20.

[25] A. Takayama, T. Kurokawa, H. Nakayama, T. Katoh, M. Nagata, Effect of Ba and La Additives to the Pd Layer of a Pd:Rh TWC, SAE Tech. Pap. (2017) 2017-01–0922. doi:10.4271/2017-01-0922.

[26] A. David Logan, G.W. Graham, NO chemisorption on Pd(100) with ultra-thin overlayers of oxidized La and Al, Surf. Sci. Lett. 277 (1992) L47–L51.

[27] S. Matsuura, A. Hirai, K. Arimura, H. Shinjoh, Development of three-way catalyst with using only Pd as

activator, SAE Tech. Pap. (1995) 950257. doi:10.4271/950257.

[28] M. Valden, R.L. Keiski, N. Xiang, J. Pere, J. Aaltonen, M. Pessa, T. Maunula, A. Savimäki, A. Lahti, M. Härkönen, Reactivity of $Pd/Al_2O_3$, $Pd/La_2O_3$-$Al_2O_3$ and $Pd/LaAlO_3$ catalysts for the reduction of NO by CO: CO and NO adsorption, J. Catal. 161 (1996) 614–625.

[29] M. Skoglundh, H. Johansson, L. Löwendahl, K. Jansson, L. Dahl, B. Hirschauer, Cobalt-promoted palladium as a three-way catalyst, Appl. Catal. B Environ. 7 (1996) 299–319. http://linkinghub.elsevier.com/retrieve/pii/0926337395000496.

[30] K. Tanikawa, C. Egawa, Effect of barium addition over palladium catalyst for CO-NO-$O_2$ reaction, J. Mol. Catal. A Chem. 349 (2011) 94–99. doi:10.1016/j.molcata.2011.08.025.

[31] H. Muraki, H. Shinjoh, Y. Fujitani, Effect of lanthanum on the no reduction over palladium catalysts, Appl. Catal. 22 (1986) 325–335.

[32] H. Muraki, H. Shinjoh, H. Sobukawa, K. Yokota, Y. Fujitani, Palladium-Lanthanum Catalysts for Automotive Emission Control, Ind. Eng. Chem. Prod. Res. Dev. 25 (1986) 202–208.

[33] H. Muraki, K. Yokota, Y. Fujitani, Nitric oxide reduction performance of automotive palladium catalysts, Appl. Catal. 48 (1989) 93–105.

[34] H. Shinjoh, Rare earth metals for automotive exhaust catalysts, J. Alloys Compd. 408–412 (2006) 1061–1064.

[35] T. Sekiba, S. Kimura, H. Yamamoto, A. Okada, Development of automotive palladium three-way catalysts, Catal. Today. 22 (1994) 113–126. doi:10.1016/0920-5861(94)80096-0.

[36] T. Kobayashi, T. Yamada, K. Kayano, Effect of basic metal additives on $NO_x$ reduction property of Pd-based three-way catalyst, Appl. Catal. B Environ. 30 (2001) 287–292. doi:10.1016/S0926-3373(00)00240-X.

[37] Y. Jing, Z. Cai, C. Liu, T. Toyao, Z. Maeno, H. Asakura, S. Hiwasa, S. Nagaoka, H. Kondoh, K. Shimizu, Promotional Effect of La in the Three-Way Catalysis of La-Loaded $Al_2O_3$-Supported Pd Catalysts ($Pd/La/Al_2O_3$), ACS Catal. 10 (2020) 1010–1023. doi:10.1021/acscatal.9b03766.

[38] T. Toyao, Y. Jing, K. Kon, T. Hayama, S. Nagaoka, K. Shimizu, Catalytic NO–CO Reactions over La-$Al_2O_3$ Supported Pd: Promotion Effect of La, Chem. Lett. 47 (2018) 1036–1039. http://www.journal.csj.jp/doi/10.1246/cl.180388.

[39] H.S. Gandhi, G.W. Graham, R.W. McCabe, Automotive exhaust catalysis, J. Catal. 216 (2003) 433–442.

[40] S.B. Kang, I.S. Nam, B.K. Cho, C.H. Kim, S.H. Oh, Kinetic model for modern double-layered Pd/Rh TWC as a function of metal loadings and mileage, Chem. Eng. J. 278 (2015) 328–338. doi:10.1016/j.cej.2014.12.106.

[41] A. Fujiwara, Y. Tsurunari, H. Yoshida, J. Ohyama, T. Yamada, M. Haneda, T. Miki, M. Machida, Thermal Deactivation of $Pd/CeO_2$-$ZrO_2$ Three-Way Catalysts during Real Engine Aging: Analysis by a Surface plus Peripheral Site Model, ACS Omega. 5 (2020) 28897−28906. doi:10.1021/acsomega.0c04644.

[42] B. Ravel, M. Newville, ATHENA, ARTEMIS, HEPHAESTUS: Data analysis for X-ray absorption

spectroscopy using IFEFFIT, J. Synchrotron Radiat. 12 (2005) 537–541. doi:10.1107/S0909049505012719.

[43] T. Yamamoto, T. Hatsui, T. Matsuyama, T. Tanaka, T. Funabiki, Structures and Acid-Base Properties of La/$Al_2O_3$- Role of La Addition to Enhance Thermal Stability of γ-$Al_2O_3$, Chem. Mater. 15 (2003) 4830–4840.

[44] S.J. Smith, B. Huang, C.H. Bartholomew, B.J. Campbell, J. Boerio-Goates, B.F. Woodfield, La-Dopant Location in La-Doped γ-$Al_2O_3$ Nanoparticles Synthesized Using a Novel One-Pot Process, J. Phys. Chem. C. 119 (2015) 25053−25062. doi:10.1021/acs.jpcc.5b07256.

[45] K. Tamai, S. Hosokawa, A. Yamamoto, H. Asakura, K. Teramura, T. Tanaka, Identification of Active Ba Species on $TiO_2$ Photocatalyst for $NO_x$ Trapping, Chem. Lett. 49 (2020) 859–862. doi:10.1246/cl.200236.

[46] K. Zorn, S. Giorgio, E. Halwax, C.R. Henry, H. Grönbeck, G. Rupprechter, CO oxidation on technological Pd-$Al_2O_3$ catalysts: Oxidation state and activity, J. Phys. Chem. C. 115 (2011) 1103–1111. doi:10.1021/jp106235x.

[47] M. Gajdoš, A. Eichler, J. Hafner, CO adsorption on close-packed transition and noble metal surfaces: Trends from ab initio calculations, J. Phys. Condens. Matter. 16 (2004) 1141–1164. doi:10.1088/0953-8984/16/8/001.

[48] C.D. Zeinalipour-Yazdi, A.L. Cooksy, A.M. Efstathiou, CO adsorption on transition metal clusters: Trends from density functional theory, Surf. Sci. 602 (2008) 1858–1862. doi:10.1016/j.susc.2008.03.024.

[49] S. Gonzalez, F. Illas, CO adsorption on monometallic Pd, Rh, Cu and bimetallic PdCu and RhCu monolayers supported on Ru(0001), Surf. Sci. 598 (2005) 144–155. doi:10.1016/j.susc.2005.08.035.

[50] G. Ketteler, D.F. Ogletree, H. Bluhm, H. Liu, E.L.D. Hebenstreit, M. Salmeron, In situ spectroscopic study of the oxidation and reduction of Pd(111), J. Am. Chem. Soc. 127 (2005) 18269–18273. doi:10.1021/ja055754y.

[51] Y.N. Kim, M.Y. Kim, M. Choi, Synergistic integration of catalysis and ion-exchange for highly selective reduction of nitrate into N2, Chem. Eng. J. 289 (2016) 423–432. doi:10.1016/j.cej.2016.01.002.

[52] R. Toyoshima, K. Amemiya, K. Mase, H. Kondoh, Orientation-Dependent Hindrance to the Oxidation of Pd-Au Alloy Surfaces, J. Phys. Chem. Lett. 11 (2020) 9249–9254. doi:10.1021/acs.jpclett.0c02645.

[53] L. Zhang, I.A.W. Filot, Y.Q. Su, J.X. Liu, E.J.M. Hensen, Transition metal doping of Pd(111) for the NO + CO reaction, J. Catal. 363 (2018) 154–163. doi:10.1016/j.jcat.2018.04.025.

[54] N. Takagi, K. Ishimura, H. Miura, T. Shishido, R. Fukuda, M. Ehara, S. Sakaki, Catalysis of Cu Cluster for NO Reduction by CO: Theoretical Insight into the Reaction Mechanism, ACS Omega. 4 (2019) 2596–2609.

[55] M. Grünbacher, A. Tarjomannejad, P.D.K. Nezhad, C. Praty, K. Ploner, A. Mohammadi, A. Niaei, B. Klötzer, S. Schwarz, J. Bernardi, A. Farzi, M.J.I. Gómez, V.T. Rivero, S. Penner, Promotion of La(Cu0.7Mn0.3)0.98M0.02O3−δ (M = Pd, Pt, Ru and Rh) perovskite catalysts by noble metals for the reduction of NO by CO, J. Catal. 379 (2019) 18–32. doi:10.1016/j.jcat.2019.09.005.

[56] L. Savereide, A. Gosavi, K.E. Hicks, J.M. Notestein, Identifying properties of low-loaded CoOx/CeO2 via X-ray absorption spectroscopy for NO reduction by CO, J. Catal. 381 (2020) 355–362. doi:10.1016/j.jcat.2019.11.016.

[57] S.T. Oyama, X. Zhang, J. Lu, Y. Gu, T. Fujitani, Epoxidation of propylene with $H_2$ and $O_2$ in the explosive regime in a packed-bed catalytic membrane reactor, J. Catal. 257 (2008) 1–4. doi:10.1016/j.jcat.2008.04.023.

[58] N. Macleod, J. Isaac, R.M. Lambert, Sodium Promotion of the NO+$C_3H_6$ Reaction over Rh/γ-$Al_2O_3$ Catalysts, J. Catal. 193 (2000) 115–122. doi:10.1006/jcat.2000.2882.

[59] M. Konsolakis, I. V. Yentekakis, The reduction of NO by propene over Ba-promoted Pt/γ-$Al_2O_3$ catalysts, J. Catal. 198 (2001) 142–150. doi:10.1006/jcat.2000.3123.

[60] P.J. Berlowitz, C.H.F. Peden, D.W. Goodman, Kinetics of CO Oxidation on Single-Crystal Pd, Pt, and Ir, J. Phys. Chem. 92 (1988) 5213–5221.

[61] E.J. Peterson, A.T. DeLaRiva, S. Lin, R.S. Johnson, H. Guo, J.T. Miller, J.H. Kwak, C.H.F. Peden, B. Kiefer, L.F. Allard, F.H. Ribeiro, A.K. Datye, Low-temperature carbon monoxide oxidation catalysed by regenerable atomically dispersed palladium on alumina, Nat. Commun. 5 (2014) 4885.

[62] H. Asakura, S. Hosokawa, T. Ina, K. Kato, K. Nitta, K. Uera, T. Uruga, H. Miura, T. Shishido, J. Ohyama, A. Satsuma, K. Sato, A. Yamamoto, S. Hinokuma, H. Yoshida, M. Machida, S. Yamazoe, T. Tsukuda, K. Teramura, T. Tanaka, Dynamic Behavior of Rh Species in Rh/$Al_2O_3$ Model Catalyst during Three-Way Catalytic Reaction: An Operando X-ray Absorption Spectroscopy Study, J. Am. Chem. Soc. 140 (2018) 176–184. doi:10.1021/jacs.7b07114.

[63] D. Decarolis, A.H. Clark, T. Pellegrinelli, M. Nachtegaal, E.W. Lynch, C.R.A. Catlow, E.K. Gibson, A. Goguet, P.P. Wells, Spatial profiling of a Pd/$Al_2O_3$ catalyst during selective ammonia oxidation, ACS Catal. 11 (2021) 2141–2149. doi:10.1021/acscatal.0c05356.

[64] M. Che, J.F. Dutel, P. Gallezot, M. Primet, A study of the chemisorption of nitric oxide on PdY zeolite. Evidence for a room temperature oxidative dissolution of Pd crystallites, J. Phys. Chem. 80 (1976) 2371–2381. doi:10.1021/j100562a011.

[65] A.W. Aylor, L.J. Lobree, J.A. Reimer, A.T. Bell, Investigations of the dispersion of Pd in H-ZSM-5, J. Catal. 172 (1997) 453–462. doi:10.1006/jcat.1997.1893.

[66] K. Paredis, L.K. Ono, F. Behafarid, Z. Zhang, J.C. Yang, A.I. Frenkel, B.R. Cuenya, Evolution of the structure and chemical state of Pd nanoparticles during the in situ catalytic reduction of NO with $H_2$, J. Am. Chem. Soc. 133 (2011) 13455–13464. doi:10.1021/ja203709t.

[67] S. Yasumura, H. Ide, T. Ueda, Y. Jing, C. Liu, K. Kon, T. Toyao, Z. Maeno, K. Shimizu, Transformation of Bulk Pd to Pd Cations in Small-Pore CHA Zeolites Facilitated by NO, JACS Au. 1 (2021) 201–211. doi:10.1021/jacsau.0c00112.

[68] P.T. Fanson, M.R. Horton, W.N. Delgass, J. Lauterbach, FTIR analysis of storage behavior and sulfur tolerance in barium-based NOx storage and reduction (NSR) catalysts, Appl. Catal. B Environ. 46 (2003) 393–413. doi:10.1016/S0926-3373(03)00275-3.

[69] K. Fujiwara, S.E. Pratsinis, Single Pd atoms on $TiO_2$ dominate photocatalytic $NO_x$ removal, Appl. Catal.

B Environ. 226 (2018) 127–134. doi:10.1016/j.apcatb.2017.12.042.

[70] W.A. Brown, D.A. King, NO Chemisorption and Reactions on Metal Surfaces: A New Perspective, J. Phys. Chem. B. 104 (2000) 2578–2595. doi:10.1021/jp9930907.

[71] C. Sedlmair, K. Seshan, A. Jentys, J.A. Lercher, Elementary steps of NOx adsorption and surface reaction on a commercial storage-reduction catalyst, J. Catal. 214 (2003) 308–316. doi:10.1016/S0021-9517(02)00085-4.

[72] I. Nova, L. Castoldi, L. Lietti, E. Tronconi, P. Forzatti, F. Prinetto, G. Ghiotti, NOx adsorption study over Pt-Ba/alumina catalysts: FT-IR and pulse experiments, J. Catal. 222 (2004) 377–388. doi:10.1016/j.jcat.2003.11.013.

[73] Y. Chi, S.S.C. Chuang, Infrared and TPD Studies of Nitrates Adsorbed on $Tb_4O_7$, $La_2O_3$, BaO, and MgO/y-$Al_2O_3$, J. Phys. Chem. B. 104 (2000) 4673–4683. http://linkinghub.elsevier.com/retrieve/pii/S0360319915012847.

[74] L. Lietti, M. Daturi, V. Blasin-Aubé, G. Ghiotti, F. Prinetto, P. Forzatti, Relevance of the Nitrite Route in the NOx Adsorption Mechanism over Pt-Ba/$Al_2O_3$ $NO_x$ Storage Reduction Catalysts Investigated by using Operando FTIR Spectroscopy, ChemCatChem. 4 (2012) 55–58.

[75] A.G. Greenaway, A. Marberger, A. Thetford, I. Lezcano-González, M. Agote-Arán, M. Nachtegaal, D. Ferri, O. Kröcher, C.R.A. Catlow, A.M. Beale, Detection of key transient Cu intermediates in SSZ-13 during $NH_3$-SCR deNOx by modulation excitation IR spectroscopy, Chem. Sci. 11 (2020) 447–455. doi:10.1039/c9sc04905c.

[76] I.S. Pieta, M. García-Diéguez, C. Herrera, M.A. Larrubia, L.J. Alemany, In situ DRIFT-TRM study of simultaneous NOx and soot removal over Pt-Ba and Pt-K NSR catalysts, J. Catal. 270 (2010) 256–267.

[77] M. Haneda, Y. Kintaichi, I. Nakamura, T. Fujitani, H. Hamada, Effect of surface structure of supported palladium catalysts on the activity for direct decomposition of nitrogen monoxide, J. Catal. 218 (2003) 405–410.

[78] F. Frola, M. Manzoli, F. Prinetto, G. Ghiotti, L. Castoldi, L. Lietti, Pt-Ba/$Al_2O_3$ NSR catalysts at different ba loading: Characterization of morphological, structural, and surface properties, J. Phys. Chem. C. 112 (2008) 12869–12878. doi:10.1021/jp801480t.

[79] H. Shinjoh, N. Isomura, H. Sobukawa, M. Sugiura, Effect of Alkaline Addition on Hydrocarbon Oxidation Activities of Palladium Three-way Catalyst, Stud. Surf. Sci. Catal. 116 (1998) 83–91.

[80] I. Friberg, N. Sadokhina, L. Olsson, Complete methane oxidation over Ba modified Pd/$Al_2O_3$: The effect of water vapor, Appl. Catal. B Environ. 231 (2018) 242–250. doi:10.1016/j.apcatb.2018.03.003.

[81] J. Gong, D. Wang, J. Li, N. Currier, A. Yezerets, Dynamic oxygen storage modeling in a three-way catalyst for natural gas engines: A dual-site and shrinking-core diffusion approach, Appl. Catal. B Environ. 203 (2017) 936–945. doi:10.1016/j.apcatb.2016.11.005.

[82] M. Machida, A. Fujiwara, H. Yoshida, J. Ohyama, H. Asakura, S. Hosokawa, T. Tanaka, M. Haneda, A. Tomita, T. Miki, K. Iwashina, Y. Endo, Y. Nakahara, S. Minami, N. Kato, Y. Hayashi, H. Goto, M. Hori, T. Tsuda, K. Miura, F. Kimata, K. Iwachido, Deactivation Mechanism of Pd/$CeO_2$-$ZrO_2$ Three-Way

Catalysts Analyzed by Chassis-Dynamometer Tests and in Situ Diffuse Reflectance Spectroscopy, ACS Catal. 9 (2019) 6415−6424. doi:10.1021/acscatal.9b01669.

[83] T. Okajima, S. Sivakumar, H. Shingyouchi, K. Yamaguchi, J. Kusaka, M. Nagata, Modeling on a Three-Way Catalyst Used in Series Hybrid Electric Vehicles Considering Its Specific Engine Operation Attribute, Ind. Eng. Chem. Res. 60 (2021) 1583−1601. doi:10.1021/acs.iecr.0c05436.

[84] A.K. Datye, M. Votsmeier, Opportunities and challenges in the development of advanced materials for emission control catalysts, Nat. Mater. (2020). doi:10.1038/s41563-020-00805-3.

[85] M. Haneda, Y. Nakamura, T. Yamada, S. Minami, N. Kato, K. Iwashina, Y. Endo, Y. Nakahara, K. Iwachido, Comprehensive study of the light-off performance and surface properties of engine-aged Pd-based three-way catalysts, Catal. Sci. Technol. 11 (2021) 912–922. doi:10.1039/d0cy01952f.

## Graphical Abstract